Materials Chemistry and Physics 137 (2012) 359–364

Contents lists available at SciVerse ScienceDirect

Materials Chemistry and Physics

journal homepage: www.elsevier.com/locate/matchemphys

Single domain limit for $Ni_xCo_{1-x}Fe_2O_4$ ($0 \leq x \leq 1$) nanoparticles synthesized by coprecipitation route

K. Maaz [a,b], Gil-Ho Kim [a,*]

[a] School of Electronic and Electrical Engineering and Sungkyunkwan Advanced Institute of Nanotechnology (SAINT), Sungkyunkwan University, Suwon 440-746, Republic of Korea
[b] Nanomaterials Research Group, Physics Division, PINSTECH, Nilore 45650, Islamabad, Pakistan

HIGHLIGHTS

- $Ni_xCo_{1-x}Fe_2O_4$ ($0 \leq x \leq 1$) nanoparticles have been synthesized by co-precipitation route.
- Coercivity has been studied as a function particle size for various nickel concentrations (x).
- Single domain limit (d_{sdl}) for the nanoparticles was found to vary linearly with x.
- Blocking temperature and saturation magnetization show increasing trends with increasing x.

GRAPHICAL ABSTRACT

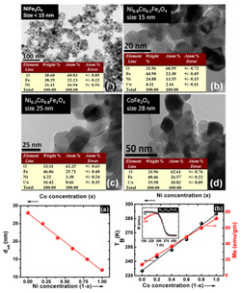

ARTICLE INFO

Article history:
Received 18 June 2012
Received in revised form
9 September 2012
Accepted 17 September 2012

Keywords:
Magnetic materials
Electron microscopy
Annealing
Hysteresis
Magnetic properties

ABSTRACT

$Ni_xCo_{1-x}Fe_2O_4$ ($0 \leq x \leq 1$) nanoparticles (sizes: 8–52 nm) were synthesized by chemical coprecipitation route. Single domain limit (d_{sdl}) for the nanoparticles, determined from the coercivity (H_C) versus particle-size curves, was explored as a function of nickel concentration (x). The coercivity of the particles attains a peak value at d_{sdl}, and it was found that coercivity decreases linearly with increasing nickel concentration in the samples. The saturation magnetization (M_S) and blocking temperature (T_b) of the system show increasing trends with increasing cobalt concentration in the nanoparticles.

1. Introduction

In the recent years, nanostructured materials that exhibit interesting optical, electrical, chemical, and magnetic properties have attracted considerable attention [1–3]. These properties, along-with their high chemical and physical stabilities, are of great technological interest [4–6]. The magnetic character of nanoparticles depends crucially on the size, shape, purity, and magnetic stability of these materials. These nanoparticles should be in the single-domain state with high coercivity and moderate magnetization. The most significant properties of magnetic nanoparticles, namely, magnetic saturation, coercivity, and magnetization, change drastically as the size of the particle decreases within the nanometric range [7,8]. At the nanoscale, among various magnetic materials, nickel-cobalt ferrite [$Ni_xCo_{1-x}Fe_2O_4$ ($0 \leq x \leq 1$)] possesses attractive magnetic properties for their use as a soft and hard magnet and low-loss material at high frequencies. Owing to the variation of surface-to-volume ratio of atoms at the nanoscale, particle size plays a crucial role in determining the magnetic properties of the atoms. There exists a certain critical particle size

* Corresponding author.
E-mail address: ghkim@skku.edu (G.-H. Kim).

0254-0584/$ – see front matter © 2012 Elsevier B.V. All rights reserved.
http://dx.doi.org/10.1016/j.matchemphys.2012.09.034

called the *critical single domain size* (d_{sdl}) at which all the nanoparticles are in the single-domain blocked (ferromagnetic) state. At this size the nanoparticles exhibit optimum magnetic properties and are of great importance from their application point of view.

It is difficult to attain the precise control over the size and size distribution with existing nanoparticle preparation techniques [9]. To overcome these difficulties we employed the coprecipitation method for synthesizing the nanoparticles. In this method, nanometer-sized reactors are used for synthesizing homogeneous $Ni_xCo_{1-x}Fe_2O_4$ ($0 \le x \le 1$) nanoparticles. The prepared particles are coated with a surfactant [10,11] and then dispersed in a carrier liquid (ethanol, methanol, ammonia) in order to protect their oxidation in the presence of atmospheric oxygen. In this method, the production rate of ferrite nanoparticles is high, and the control over the size and size distribution is relatively easy. We report synthesis of $Ni_xCo_{1-x}Fe_2O_4$ ($0 \le x \le 1$) nanoparticles by the chemical coprecipitation method and explore d_{sdl} based on the study of coercivity as function of particle size (d) and doping concentration x. This is a detailed study reporting d_{sdl} for this particular series of ferrite nanoparticles.

2. Experimental details

We used nickel-, cobalt-, and ferric-chloride (each with purity of 99.99%, Aldrich), NaOH (GR, 28–30%), and oleic acid (Albright and Wilson Asia Pvt. Ltd., Singapore) for synthesizing $Ni_xCo_{1-x}Fe_2O_4$ ($0 \le x \le 1$) nanoparticles. Three molar (M) NaOH was mixed with 0.4 M ferric chloride and 0.2 M nickel- and cobalt-chloride. The pH of the solution was maintained at 12. Few drops (3–4) of oleic acid were added to the solution as the surfactant before starting the reaction at 80 °C for approximately 50 min. The product was then cooled to room temperature and washed with water and ethanol in sequence to ensure the removal of uncreative water soluble ions and extra surfactant molecules. The mixture was centrifuged for 10 min at 2000 rpm and then dried overnight at temperature of 80 °C. The acquired substance was then grinded into the fine powders and then annealed for 6 h at 600–1000 °C. It has been reported earlier that the particle size increases with increasing annealing temperature [12]. In this work we have obtained larger sizes by annealing the samples at high temperatures. High temperature annealing generally decreases the lattice defects and strains and causes coalescence of crystallites that results in the increasing size of the nanoparticles [12,13].

The following reaction was followed synthesizing the nanoparticles;

$$x\mathrm{NiCl_2}\cdot 6\mathrm{H_2O(aq)} + (1-x)\mathrm{CoCl_2}\cdot 6\mathrm{H_2O(aq)} + \mathrm{FeCl_3}\cdot 6\mathrm{H_2O(aq)} + \mathrm{NaOH(aq)} + \text{Oleic acid(l)} \rightarrow \text{Oleic acid coated } \mathrm{Ni_xCo_{1-x}Fe_2O_4}\ (0 \le x \le 1)(\mathrm{s}) + \mathrm{NaCl(aq)} + \text{oleic acid (l) [unused]} + \mathrm{H_2O(l)}$$

The reaction kinetics mainly depend upon the nucleation and growth processes. Particle size and size-distribution can be controlled by controlling the relative rates of these two processes. If the nucleation rate is high than the growth rate then smaller particles with small size-distribution are obtained. On the other hand if the growth rate is high than the nucleation rate then larger particles with large size-distribution are achieved. During the reaction these two processes are generally optimized by the controlled addition of NaOH.

Structural characterization was performed by X-ray diffractometer (Model: X'Pert Philips, with Cu-Kα $\lambda = 0.154056$ nm) and high-resolution transmission electron microscope (HRTEM, JEM-3010). The average particle size was calculated from the line broadening of the (311) peak of the XRD using the well-known Debye–Scherrer equation [14]. The particle size was cross-checked using the results of TEM and it was found in good agreement with the XRD results. Particle-size distribution was determined from TEM analysis, which was found to be within a limit of ±9%.

Magnetic characterization was performed using vibrating sample magnetometer (VSM, Model 7300 Lake Shore) with an applied field of ±10 kOe. The powder nanoparticles were compressed to form hard pellets for the VSM measurements. No further heat treatment of the pellet was carried out during sample preparation for magnetic measurements, because high-temperature heat treatment can affect (increase) the particle size. Notably, the high-temperature (>600 °C) annealing carried out during the synthesis process removed the surfactant from the prepared particles. This decreases the inter-particle distance to the extent where the nanoparticles could interact strongly through the exchange and dipole–dipole magnetic interactions. In such cases, it is important to include these contributions while characterizing the magnetic results of the samples.

3. Results and discussion

TEM images of four samples ($NiFe_2O_4$, $Ni_{0.8}Co_{0.2}Fe_2O_4$, $Ni_{0.2}Co_{0.8}Fe_2O_4$, and $CoFe_2O_4$) are shown in Fig. 1(a)–(d) with average particle sizes of 12, 15, 25, and 28 nm. In these images, most particles appear to have the spherical shape; however, some elongated particles can also be seen in the samples. The particle size was controlled by the relative rate of nucleation and growth during the reaction. Whereas, during the annealing process the particle size was controlled by the annealing temperature of the samples. Smaller and uniformly distributed particles are obtained if the nucleation rate is higher than the growth rate, whereas the high annealing temperature causes an increase in the particle size due to the coalescence, resulting in an increasing grain size of the samples [12,13]. The energy dispersive spectroscopy (EDS) results of the same samples ($NiFe_2O_4$, $Ni_{0.8}Co_{0.2}Fe_2O_4$, $Ni_{0.2}Co_{0.8}Fe_2O_4$, and $CoFe_2O_4$) obtained from TEM analysis are tabulated in the inset of Fig. 1. The EDS data was taken using standard-less quantitative analysis software. This software utilizes fundamental parameter (FP) methods for quantitative analysis as the standards. This allows the quantitative and qualitative analyses of the samples such as metals, alloys, and oxides. The EDS results shown in Fig. 1 give the qualitative composition of the samples as well as the presence of Co, Ni, Fe, and oxygen in the nanoparticles. Fig. 1 confirms the weight- and atomic-percentages of Ni and Co present in the samples. These results can be used to calculate the nickel concentration (x) in the samples which we were found be 1.0, 0.8, 0.6, 0.4, 0.2, and 0. Moreover, the EDS analysis shows that there are no impurities present in the samples. Fig. 2 shows the XRD results of four samples ($NiFe_2O_4$, $Ni_{0.8}Co_{0.2}Fe_2O_4$, $Ni_{0.2}Co_{0.8}Fe_2O_4$, and $CoFe_2O_4$); with all the peaks correspond to the inverse spinel structure. These peaks are the result of pure-phase Ni- and Co-ferrite, which can be indexed according to JCPDS cards (# 742081 for Ni-ferrite and # 791744 for Co-ferrite), thereby confirming their pure phase and inverse spinel structure.

$M(H)$ loops of the samples obtained at room temperature performed under an applied field of ±10 kOe are shown in Fig. 3. From these loops, the coercivity values are calculated and plotted as a function of particle size, as shown in Fig. 4. To extract the data for Fig. 4 we have prepared a series of 6 different samples with same composition and different particle sizes, and then performed their XRD and $M(H)$ analyses. These analyses for one of the samples (pure $CoFe_2O_4$) are shown in Fig. 5. In Fig. 4 it is seen that initially H_C increases with d, attains certain maximum value at d_{sdl}, and then decreases with further increasing d. The initial increase of H_C with

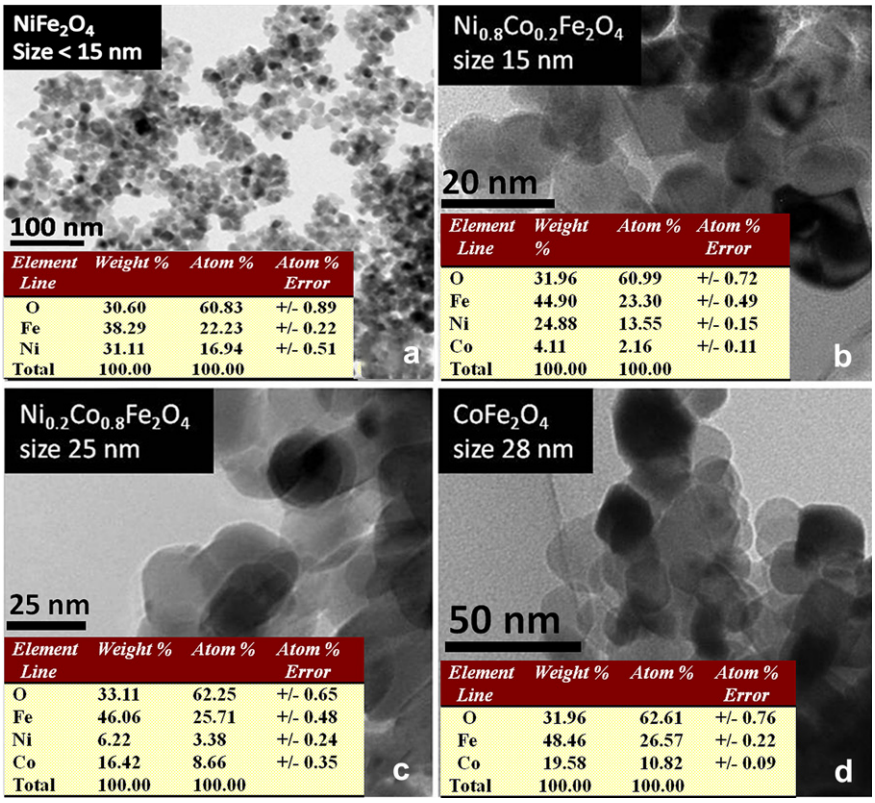

Fig. 1. TEM images of (a) 12-nm $NiFe_2O_4$ (b) 15-nm $Ni_{0.8}Co_{0.2}Fe_2O_4$ (c) 25-nm $Ni_{0.2}Co_{0.8}Fe_2O_4$, and (d) 28-nm $CoFe_2O_4$ nanoparticles synthesized by coprecipitation. The inset tables show the corresponding EDS results of the nanoparticles.

increasing d, below the peak, is assigned to the departure from the superparamagnetic state, i.e. from the unblocked to blocked (ferrimagnetic) state [15]. This phenomenon occurs for the nanoparticles with smaller d when the thermal energy (k_BT) dominates the volume-dependent anisotropy energy ($K_{eff}V$) of the system. Hence, in the lower d region, H_C increases with increasing d, because $Co_{1-x}Ni_xFe_2O_4$ ($0 \le x \le 1$) nanoparticles with larger d are expected to exhibit the ferrimagnetic blocked state. At d_{sdl} all the

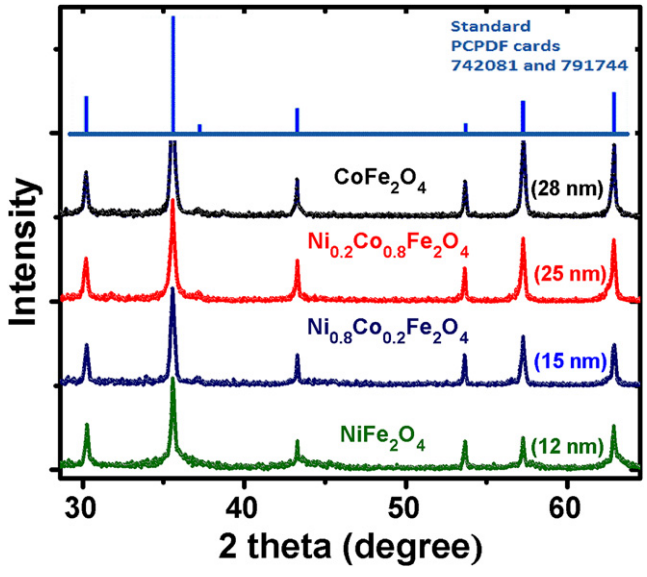

Fig. 2. XRD results of samples ($NiFe_2O_4$, $Ni_{0.8}Co_{0.2}Fe_2O_4$, $Ni_{0.2}Co_{0.8}Fe_2O_4$, and $CoFe_2O_4$), with particle size calculated from (311) peak using Debye–Scherrer equation.

nanoparticles exhibit a typical (ferrimagnetic) blocking behavior, which results in the coercivity attaining a peak value according to the Stoner–Wohlfarth model for single-domain ferromagnetic nanoparticles [16]. The decline in H_C with increasing d, above the peak, mainly occurs according to two different mechanisms. Firstly, with increasing d, the particle size becomes sufficiently large such that it can sustain the domain wall, and the magnetization reversal occurs through the domain wall motion that lowers the coercivity of the nanoparticles [17,18]. With further increasing d, this effect (of multi-domain formation) becomes more pronounced, which decreases H_C of the samples, and thus minimum H_C is achieved for the larger nanoparticles. Secondly, we consider the varying role of the surface and bulk anisotropies in larger nanoparticles. With increasing d (above the peak), the role of the surface and its associated anisotropy energy becomes more significant. It has been reported earlier that for spherical nanoparticles, the effective anisotropy constant (K_{eff}) varies with d as $K_{eff} = K_V + (6/d)K_S$ [19,20]. If we assume a similar behavior for our nanoparticles, i.e. a decrease in K_{eff} with increasing d, above the peak, it would result in the decreasing H_C of the samples that is consistent with our data (see Fig. 4). At $d = d_{sdl}$ the value of K_{eff} is maximum and the coercivity attains a peak value, as shown in Fig. 4 consistent with the Stoner–Wohlfarth model ($H_C = 2K/M_S$) as discussed above. For particles below d_{sdl}, the thermal energy is sufficient to overcome the anisotropy energy (owing to the smaller particle's volume), enabling the easier reversal of moments and thus resulting in the lower H_C values for smaller nanoparticles [21,22]. It is possible that if d is further decreased, which is not the part of this study is; the coercivity of the samples will become negligible. This is because at that point, all the nanoparticles would be in the superparamagnetic unblocked state owing to the smaller volume-dependent anisotropy energy as compared to the thermal energy of the system.

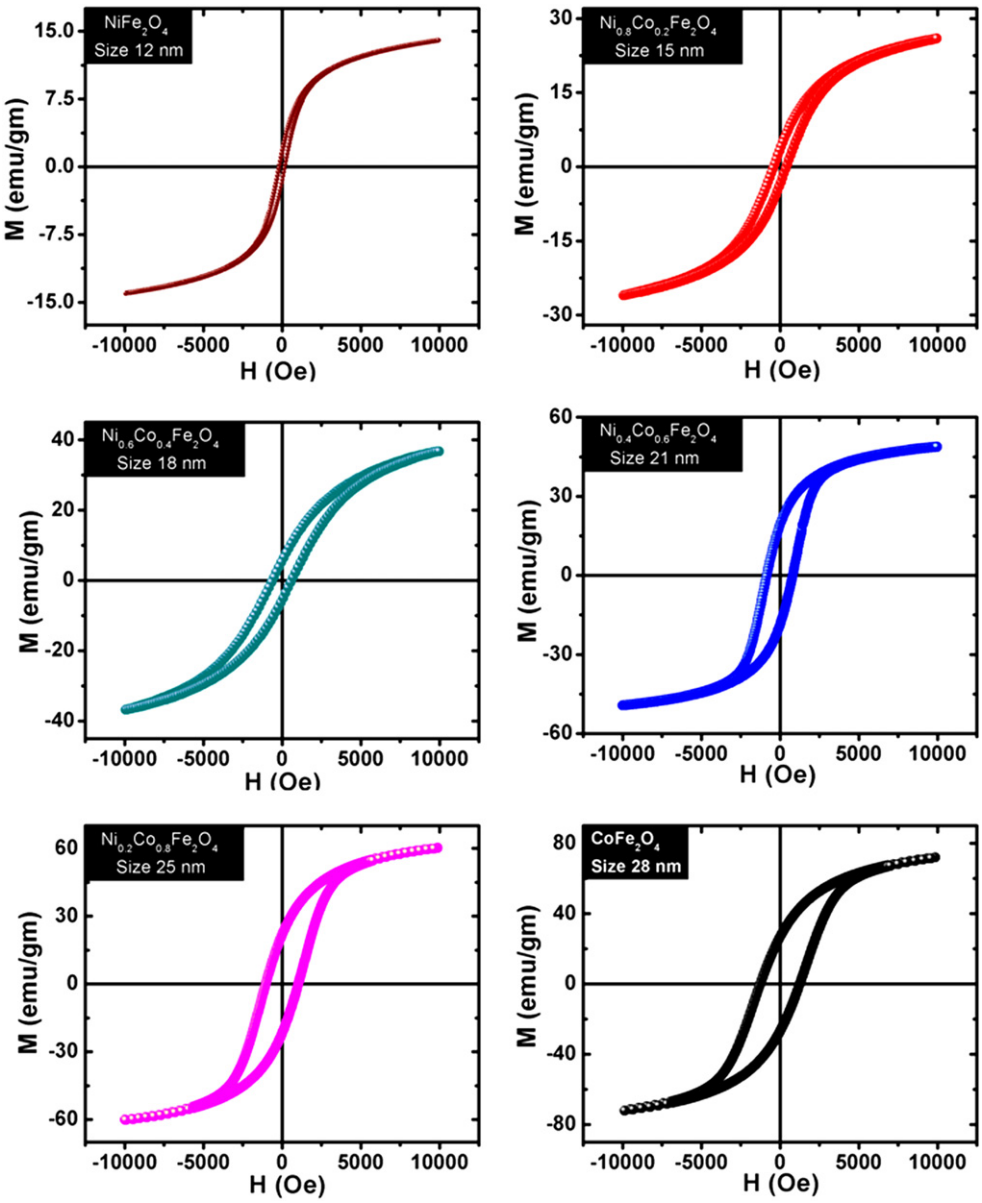

Fig. 3. Hysteresis loops for $Ni_xCo_{1-x}Fe_2O_4$ with $x = 1.0$, 0.8, 0.6, 0.4, 0.2, and 0 obtained at room temperature (300 K) under an applied field of 10 kOe.

Fig. 6(a) shows the variation of d_{sdl} with the value of x, which shows a decreasing trend of d_{sdl} as x increases. These values along with H_C are presented in Table 1. The particles sizes used in this study were determined from TEM images of the samples that were in agreement with XRD results. The decreasing trends of d_{sdl} with increasing x are due to the fact that $CoFe_2O_4$ is a hard magnetic material with high anisotropy as compared to $NiFe_2O_4$. Thus, for lower Ni concentrations the high anisotropy $CoFe_2O_4$ leads to the higher d_{sdl} values. As x increases, the overall anisotropy of the particles decreases due to the increasing content of nickel with smaller anisotropy compared to cobalt, which decreases the overall d_{sdl} of the nanoparticles.

The saturation magnetization (M_S) at 10 kOe is plotted as a function of x (red line) in Fig. 6(b). The particle size for this analysis was kept uniform (25 ± 3 nm). It is known that Ni^{+2}, Co^{+2}, Fe^{+3} ions have a magnetic moment of $2\mu_B$, $3\mu_B$, and $5\mu_B$ respectively. In $Ni_xCo_{1-x}Fe_2O_4$ ($0 \le x \le 1$) nanoparticles Fe^{+3} ions are equally distributed in tetrahedral and octahedral sites, while Ni^{+2} and Co^{+2} ions are present at the octahedral sites, which makes them fully inverse spinel ferrites [23,24]. This gives a net magnetic moment of $2\mu_B$ per molecule for $NiFe_2O_4$, $[2(x) + 3(1-x)]\mu_B$ for $Ni_xCo_{1-x}Fe_2O_4$, and $3\mu_B$ for $CoFe_2O_4$. Thus, the increasing x (and hence the decreasing cobalt concentration) lowers the overall M_S of the samples [25]. It is seen that M_S in case of $Ni_xCo_{1-x}Fe_2O_4$ ($0 \le x \le 1$) nanoparticles is appreciably smaller than the corresponding bulk values for these materials. This is attributed to the surface effects in nanoparticles or the presence of a dead/inert layer at the surface of the nanoparticles, which prevents the core-spins aligning along the field direction thereby causing a reduced M_S at the nanoscale [12,26]. The blocking temperature (T_b) calculated from the $M(T)$ curves is plotted against x as shown in Fig. 6(b). One of the representative $M(T)$ curves for $Ni_{0.2}Co_{0.8}Fe_2O_4$ is shown in the inset of the figure. For a single nanoparticle the ferromagnetically aligned magnetic moments fluctuate between their two energetically degenerate ground states on a time scale given by [27];

$$\tau = \tau_0 \exp\left(K_{eff} V_P / K_B T\right)$$

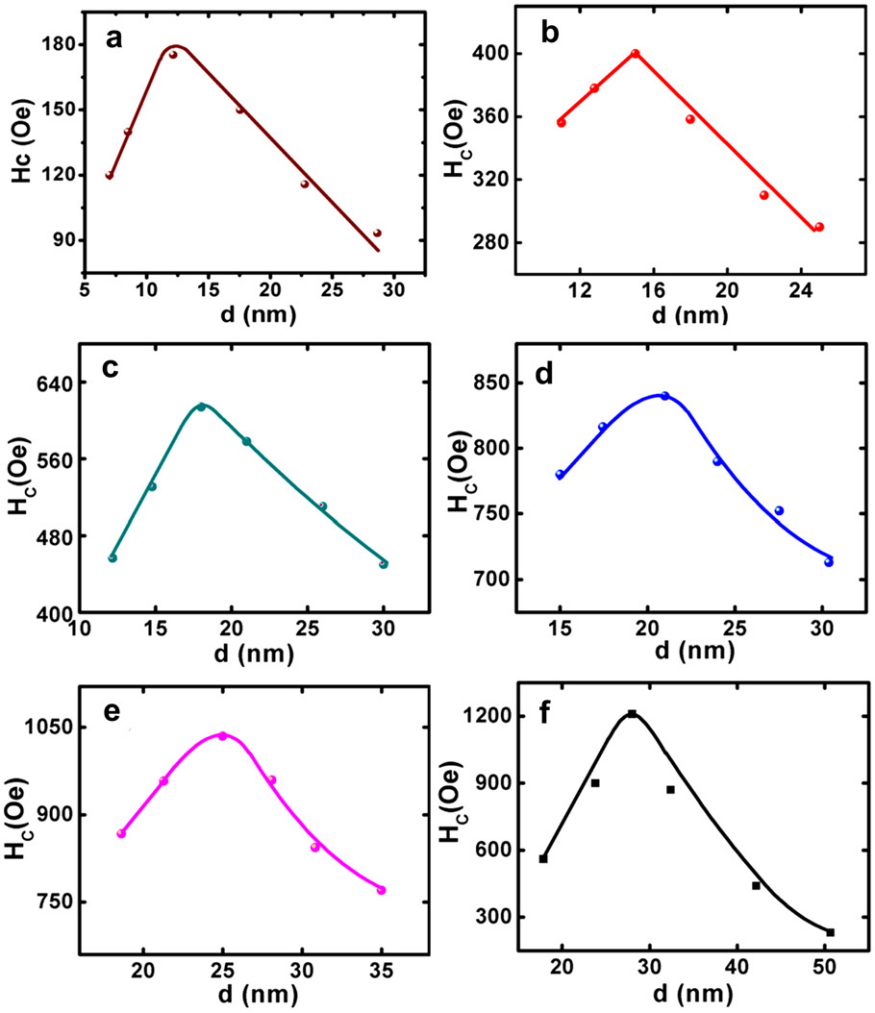

Fig. 4. Room-temperature coercivity of samples [(a) $NiFe_2O_4$, (b) $Ni_{0.8}Co_{0.2}Fe_2O_4$, (c) $Ni_{0.6}Co_{0.4}Fe_2O_4$, (d) $Ni_{0.4}Co_{0.6}Fe_2O_4$, (e) $Ni_{0.2}Co_{0.8}Fe_2O_4$, (f) $CoFe_2O_4$] as a function of particle size. H_C is calculated from the $M(H)$ loops of the samples.

where τ, K_{eff}, and V_P are the relaxation time, anisotropy constant, and volume of nanoparticles. The blocking temperature T_b is the temperature at which $\tau = \tau_m$ (the measurement time of the instrument). For a finite temperature (T) greater than T_b the nanoparticles behave in the superparamagnetic unblocked state. On the other hand, for T less than T_b the particles are in the ferromagnetic blocked state. Fig. 6(b) shows a decreasing behavior of T_b with increasing x, which is consistent with the decreasing anisotropy of the system, as the content of low-anisotropy material (i.e., Ni) increases in the system. The lower anisotropy of the system increases the probability of a jump across the anisotropy barrier, and hence the blocking is shifted toward the lower temperatures. It

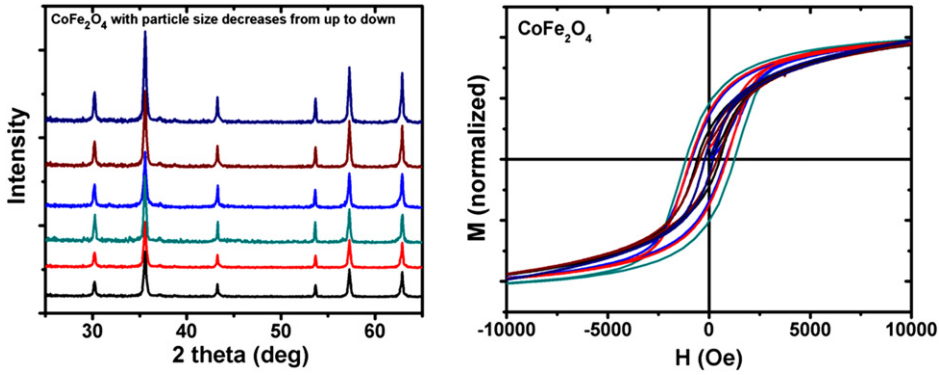

Fig. 5. (a) Represents the XRD data for 18, 24, 28, 32, 42, and 52 nm $CoFe_2O_4$ nanoparticles while (b) shows the $M(H)$ loops for these samples with normalized magnetization at 10 kOe.

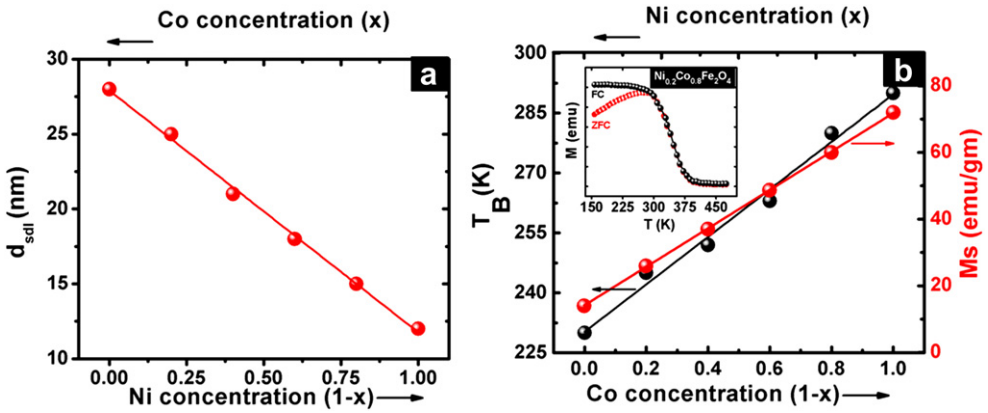

Fig. 6. (a) Correlation between single domain limit and nickel concentration. (b) Blocking temperature (black line) and saturation magnetization (red line) as a function of the samples' cobalt concentration. Inset in Fig. 6(b) shows $M(T)$ curve for one of the samples. (For interpretation of the references to colour in this figure legend, the reader is referred to the web version of this article.)

Table 1
Coercivity and single domain limit for nickel-doped cobalt ferrite nanoparticles.

	H_C (Oe)	d_{sdl} (nm)
$CoFe_2O_4$	1258	28
$Ni_{0.2}Co_{0.8}Fe_2O_4$	1035	25
$Ni_{0.4}Co_{0.6}Fe_2O_4$	830	21
$Ni_{0.6}Co_{0.4}Fe_2O_4$	612	18
$Ni_{0.8}Co_{0.2}Fe_2O_4$	405	15
$NiFe_2O_4$	178	12

is seen in the inset of Fig. 6(b) that the ZFC peak is broad, which is usually due to the large size distribution or due to the presence of interparticle dipole–dipole interactions in the samples. Both possibilities exist in our samples; however, the broadness of the peak can be ascribed mainly to the contribution of exchange and dipolar interactions in our case, as these nanoparticles are sintered together (this can be observed in TEM images). Thus in this case, T_b corresponds to the overall blocking behavior of the nanoparticle assembly as a whole, rather than the superparamagnetic blocking temperature of the isolated (non-interacting) nanoparticles. However, the actual superparamagnetic blocking temperature is expected to be proportional to T_b of the nanoparticles.

4. Conclusion

$Ni_xCo_{1-x}Fe_2O_4$ ($0 \leq x \leq 1$) nanoparticles were synthesized by chemical co-precipitation method, and various magnetic properties of these particles were explored as a function of d and x. d_{sdl} was found to decrease with increasing x, which was attributed to the overall decrease in the anisotropy of the system as the concentration of Ni increases in the samples. The decreasing trend of T_b with increasing x was assigned to the decrease of overall anisotropy of the system as the concentration of the soft phase (i.e., Ni) increased in the nanoparticles. Whereas, the decrease in M_S with increasing x is due to Ni that has relatively low magnetic moment as compared to that of cobalt.

Acknowledgments

This research was supported by the World Class University (WCU) program funded by the Ministry of Education, Science and Technology through the National Research Foundation of Korea (R32-10204).

References

[1] T.M. Whitney, J.S. Jiang, P.C. Searson, C.L. Chien, Science 261 (1993) 1316.
[2] M. Dariel, L.H. Bennett, D.S. Lashmore, P. Lubitz, M. Rubinstein, W.L. Lechter, M.Z. Harford, J. Appl. Phys. 61 (1987) 4067.
[3] W.D. Williams, N. Giordano, Phys. Rev. B 33 (1986) 8146.
[4] C.J. Brumlik, C.R. Martin, Anal. Chem. 59 (1992) 2625.
[5] S.K. Chakarvarti, J. Vetter, Nucl. Instrum. Methods B 62 (1991) 109.
[6] S.K. Chakarvarti, J. Vetter, J. Micromech. Microeng. 3 (1993) 57.
[7] D.D. Awschalom, D.P.D. Vincenzo, Phys. Today 43 (1995).
[8] I.M.L. Billas, A. Chatelain, W.A. de Heer, Science 265 (1994) 1682.
[9] V. Pallai, D.O. Shah, J. Magn. Magn. Mater. 163 (1996) 243.
[10] C. Liu, A.J. Rondinone, Z.J. Zhang, Pure Appl. Chem. 72 (1–2) (2000) 37.
[11] T. Feried, G. Shemer, G. Markovich, Adv. Mater. 13 (15) (2001) 1158.
[12] K. Maaz, A. Mumtaz, S.K. Hasanain, A. Ceylan, J. Magn. Magn. Mater. 308 (2007) 289.
[13] T.P. Raming, A.J.A. Winnubst, C.M. van Kats, P. Philipse, J. Colloid Interface Sci. 249 (2002) 346.
[14] T. Fukui, C. Sakurai, M. Okuyama, J. Mater. Res. 7 (1992) 791.
[15] K. Maaz, S. Karim, A. Mumtaz, S.K. Hasanain, J. Liu, J.L. Duan, J. Magn. Magn. Mater. 321 (2009) 1838.
[16] E.C. Stoner, E.P. Wohlfarth, IEEE Trans. Magn. 27 (1991) 3475.
[17] A.E. Berkowitz, W.J. Schuele, J. Appl. Phys. 30 (1959) 1345.
[18] W.W. Schuele, Y.D. Deet Screek, W.W. Kuhn, H. Lamprey, C. Scheer (Eds.), Ultrafine Particles, Wiley, New York, 1963, p. 218.
[19] F. Bodker, S. Morup, S. Linderoth, Phys. Rev. Lett. 72 (1994) 282.
[20] B.R. Pujada, E.H.C.P. Sinnecker, A.M. Rossi, A.P. Guimaraes, J. Appl. Phys. 93 (2003) 7217.
[21] H. Pfeiffer, Phys. Status Solidi (a) 118 (1990) 295.
[22] R. Christy, Z. Vestal, Zhang John, Nanoletters 3 (1) (2003) 1739.
[23] A. Kale, S. Gubbala, R.D.K. Misra, J. Magn. Magn. Mater. 277 (2004) 350.
[24] E.C. Sousa, M.H. Sousa, G.F. Goya, H.R. Rechenberg, M.C.F.L. Lara, F.A. Tourinho, J. Depeyrot, J. Magn. Magn. Mater. 272–276 (2004) e1215.
[25] K. Maaz, W. Khalid, A. Mumtaz, S.K. Hasanain, J. Liu, J.L. Duan, Physica E 41 (4) (2009) 593.
[26] R.H. Kodama, A.E. Berkowitz, Phys. Rev. B 59 (1999) 6321.
[27] A. Aharoni, Introduction to the Theory of Ferromagnetism, Clarendon Press, Oxford, 1996, p. 94.